Communication

Ductile-Phase Toughening in TiB_w/Ti-Ti_3Al Metallic-Intermetallic Laminate Composites

HAO WU, BO CHENG JIN, LIN GENG, GUOHUA FAN, XIPING CUI, MENG HUANG, RODRIGO MIER HICKS, and STEVEN NUTT

The concept of ductile-phase toughening was explored in a metallic-intermetallic laminate (MIL) composite comprising alternating layers of Ti_3Al and TiB_w/Ti. The laminates, in which the TiB_w/Ti layers were intended to impart toughness to the brittle Ti_3Al, were fabricated *in situ* by hot pressing and reaction annealing. Compared with monolithic Ti_3Al, the MIL composite exhibited marked increases in both fracture toughness and tensile elongation because of stress redistribution and strain delocalization by *in situ* interfaces.

DOI: 10.1007/s11661-015-3025-y

The intermetallic compound α_2-Ti_3Al has potential as a lightweight material for high-temperature structural applications, exhibiting both high strength, and resistance to oxidation and creep. However, poor ductility and toughness at room temperature prohibit the potential applications in most fields.[1,2] Various approaches have been employed in attempts to improve the toughness of intermetallic compounds, including introducing particles, fibers, or layers of ductile inclusions.[3–7] However, for a given volume fraction, ductile phase inclusions in the laminate form provide the maximum toughening efficiency, followed by fiber and particulate inclusions.[4,6]

Metallic-intermetallic laminate (MIL) composites can be fabricated by deposition or bonding the components. Deposition techniques, involving atomic scale transport of the component materials, are relatively costly and slow, and thus are not practical for production of large-scale components.[8,9] In contrast, reaction bonding of metallic foils afford multiple advantages, in particular the generation of well-bonded interfaces between the metal and the intermetallic components.[10,11] Furthermore, the laminated structure of the composite allows for variations in layer thickness and volume fractions of the components simply through the selection of initial foil thickness.[4,11,12]

In the present work, we explore the concept of ductile-phase toughening of Ti_3Al by fabrication of MIL composites. In particular, we prepare MIL composites comprising alternating layers of TiB_w/Ti and Ti_3Al by reaction annealing TiB_w/Ti foils and Al foils. Compared with pure Ti, TiB_w/Ti has a greater yield strength with little sacrifice of ductility, an important attribute to satisfy the service requirements of high-temperature materials.[13] We also assess both the synthesis process and deformation behavior of the resulting TiB_w/Ti-Ti_3Al MIL composites.

The MIL composites were fabricated by an *in situ* method, in which alternating Al foils (100 μm thick) and 5 vol pct TiB_w/Ti composite foils (500 μm thick) were stacked, followed by hot pressing at 788 K (515 °C) under 75 MPa for 1.5 hours and reaction annealing under controlled temperature and pressure (Figure 1). Typical processing parameters for reaction annealing consisted of (i) an initial annealing at 943 K (670 °C) for 3 hours to consume all of Al, and (ii) a densification treatment at 1473 K (1200 °C) for 5 hours under 40 MPa to produce a fully dense TiB_w/Ti-Ti_3Al MIL composite. The dimensions of the processed samples were 30 mm × 50 mm × 4 mm. The microstructure of the MIL composite was characterized by electron channeling contrast (ECC), electron backscatter diffraction (EBSD), energy dispersive X-ray spectroscopy (EDX), and X-ray diffraction (XRD).

Single-edge notched bend (SENB) specimens ($2 \times 4 \times 20$ mm^3, ASTM E1820) with a notched depth of 2 mm parallel to the loading direction were employed to measure the fracture toughness. The load-displacement curve was acquired automatically by using an Instron-5500 Universal Testing Machine at room temperature (RT) with a crosshead rate of 0.2 mm/min. On the basis of the maximum force, F_{max}, we can calculate the value of fracture toughness by the Eqs. [1] and [2]

$$K_{IC} = \frac{F_{max} S}{B^{1/2} W^{3/2}} \times f(a/W), \quad [1]$$

$$f(a/W) = 3(a/W)^{1/2} \times \frac{1.99 - (a/W)(1 - a/W)[2.15 - 3.93(a/W) + 2.70(a/W)^2]}{2(1 + 2a/W)(1 - a/W)^{3/2}}, \quad [2]$$

where S, B, W are the span, thickness, and width of the specimen, respectively (cm), a is the length of a

HAO WU, Ph.D. Student, LIN GENG, Professor, GUOHUA FAN, Associate Professor, XIPING CUI, Researcher, and MENG HUANG, Master Student, are with the School of Materials Science and Engineering, Harbin Institute of Technology, Harbin 150001, P.R. China. Contact e-mail: ghfan@hit.edu.cn BO CHENG JIN, Ph.D. Student, RODRIGO MIER HICKS, Master Student, and STEVEN NUTT, Professor, are with the Department of Chemical Engineering and Materials Science, M.C. Gill Composites Center, University of Southern California, Los Angeles, CA 90089-0241.

Manuscript submitted March 22, 2015
Article published online June 24, 2015

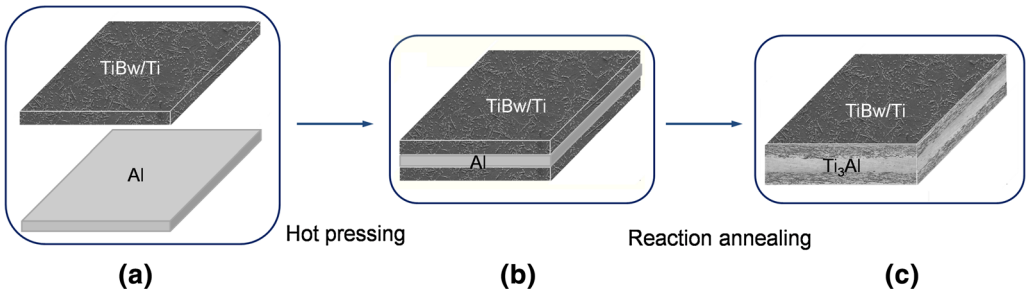

Fig. 1—Fabrication processes for TiB_w/Ti-Ti_3Al MIL composites: (*a*) stacking foils of TiB_w/Ti composite and Al; (*b*) hot pressing in vacuum to obtain TiB_w/Ti-Al laminate; (*c*) the final TiB_w/Ti-Ti_3Al MIL composite after reaction annealing.

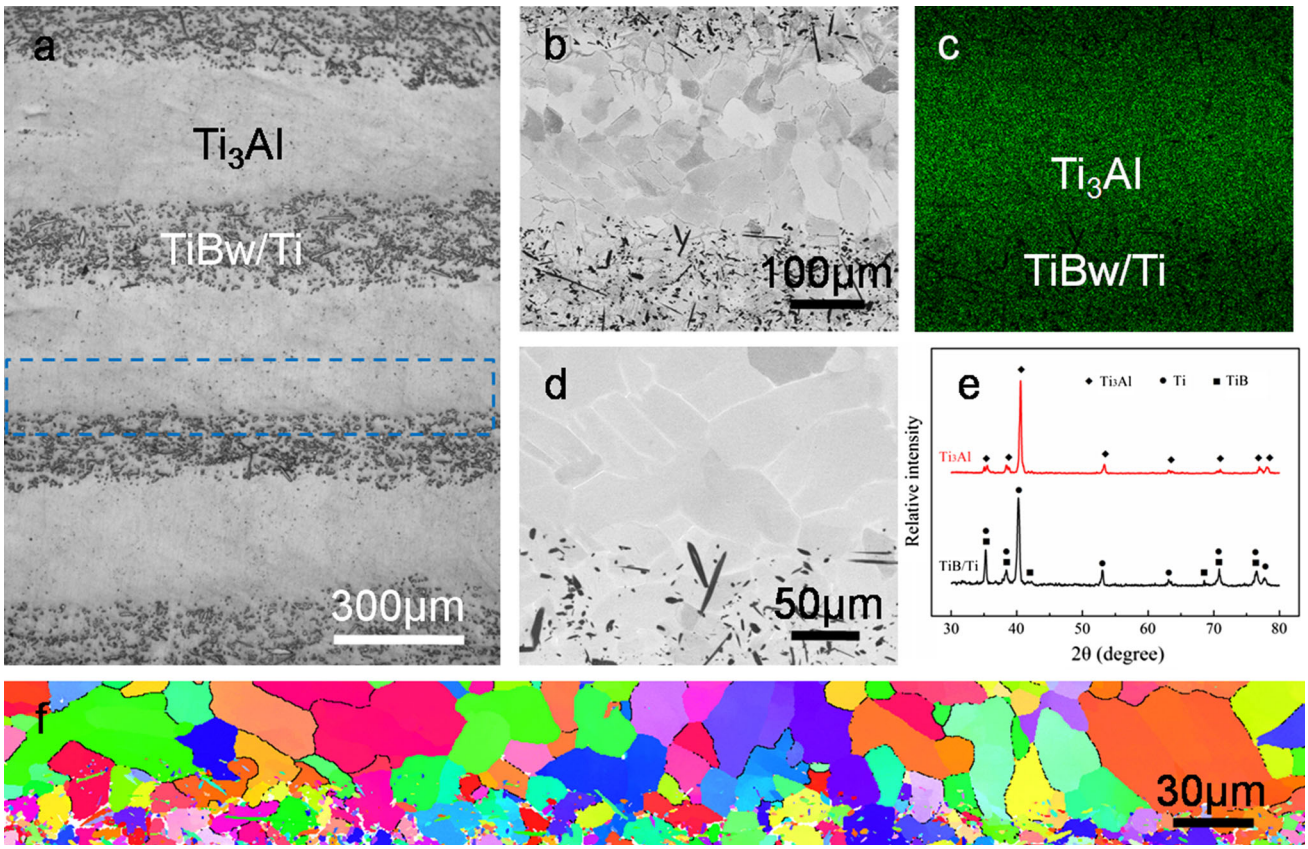

Fig. 2—Microstructure of the resulting TiB_w/Ti-Ti_3Al MIL composite: (*a*) low- and (*b*) high-magnification ECC maps showing the layered architecture, characterized by (*c*) elemental Al distribution. (b) and (*d*) show interface morphology, while (*e*) shows XRD patterns of each layer. (*f*) shows an inverse pole figure (IPF) of the interface corresponding to the regions marked in (a).

pre-crack (cm), and $f(a/W)$ is a geometry factor based on the dimension of specimens. In this work, $S = 16$ mm, $B = 2$ mm, $W = 4$ mm, $a = 2$ mm.

The tensile tests were performed at 873 K and 973 K (600 °C and 700 °C) using an Instron-1186 Universal Testing Machine with a constant strain rate of 1×10^{-4} s^{-1}. Samples were ground before testing, from 400 to 2000 grit, and then final polished by 0.5 μm diamond.

The microstructure of the MIL composites consists of alternating layers of Ti_3Al (300 μm thick) and TiB_w/Ti (150 μm thick), as shown in Figure 2. The corresponding compositions and structures are revealed by EDX (Figure 2(c)) and XRD (Figure 2(e)) results. A detailed description of the synthesis process is provided in the Supplementary Materials. Generally, in this as-fabricated composite, the hard Ti_3Al layers (coarse grain size of ~70 μm, Figures 2(d) and (f)) are expected to impart high strength and stiffness to the composites, while the TiB_w/Ti layers (fine grain size of ~10 μm) provide the desired toughness and ductility. Thus, the MIL composites are expected to be tailored to achieve an optimum combination of these two properties (strength and toughness) by adjusting the thicknesses of the original TiB_w/Ti and Al foils.

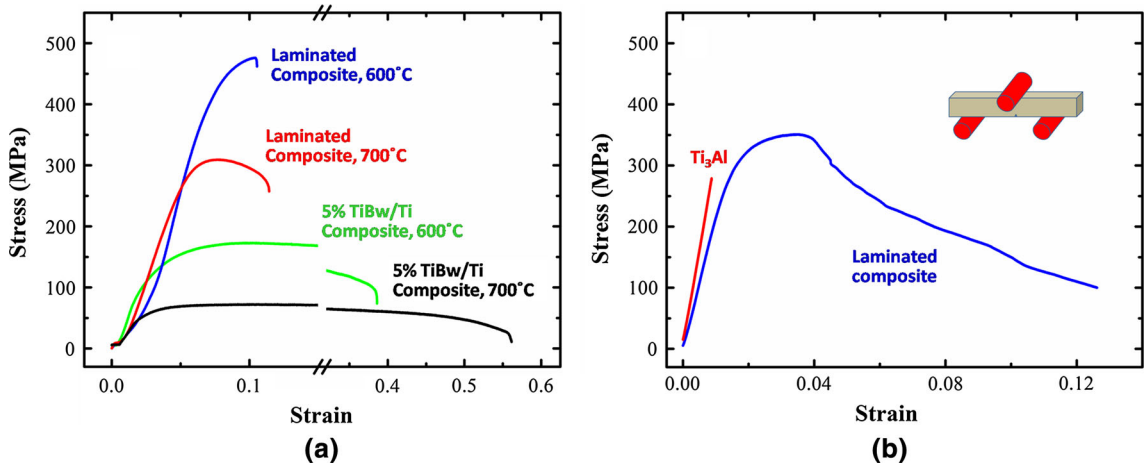

Fig. 3—(*a*) Tensile stress-strain curves and (*b*) three-point bending curves for TiB_w/Ti-Ti_3Al MIL composites, the monolithic TiB_w/Ti and Ti_3Al components.

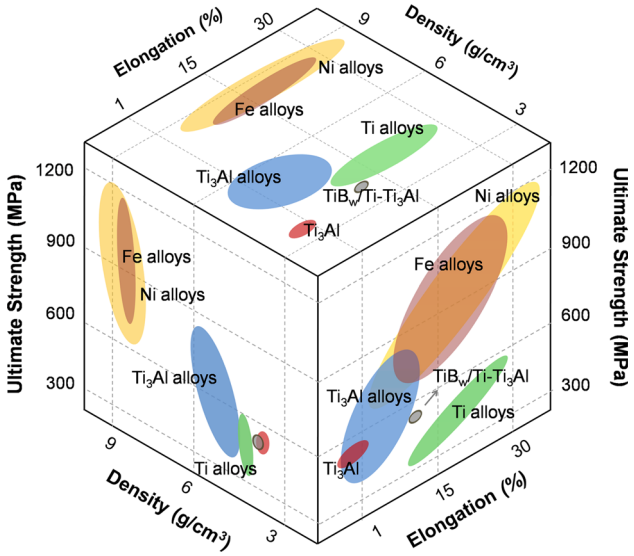

Fig. 4—Mechanical properties at 873 K (600 °C) in the high-temperature structural material family.

At high temperatures, the MIL composites exhibit tensile behavior distinct from the component layers (Figure 3(a)). In fact, the ultimate strength (σ_{UTS}) of the TiB_w/Ti-Ti_3Al MIL composite is comparable to the level of Ti_3Al-based alloys (Figure 4), despite introducing the TiB_w/Ti layer. The high strength is attributed to the role of Ti_3Al layers in the MIL composites. Generally, monolithic Ti_3Al tends to fracture in a brittle manner. However, when toughened by TiB_w/Ti, the elongation to failure (δ = 10.6 pct) at 873 K (600 °C) achieves the max value of Ti_3Al-based alloys, accompanied by a low density (lightweight compared with Ni-, Fe- and Ti_3Al-based alloys), and is about 1000 pct higher than that of monolithic Ti_3Al (Figure 4). Effectively, the brittle Ti_3Al endures relatively large strains when integrated into a laminated architecture and constrained between two ductile layers, and thus the ductile phase is not solely responsible for strain accommodation (or plastic strain). The *in situ* interface is key to the observed behavior, affording stress redistribution and preventing strain localization. Previous studies of MIL composites have reached similar conclusions.[4,14,15] As tensile deformation progresses, failure of the Ti_3Al layer removes the constraint on the TiB_w/Ti layer, and enables an extensive capacity of strain accommodation of the latter, resulting in significant plastic energy dissipation.[4,14] Moreover, TiB_w introduced during synthesis (Figure S1) refines grains in the TiB_w/Ti layers (decreasing from 100 to 10 μm), enhancing the high-temperature plasticity of the TiB_w/Ti layers.[13]

Figure 3(b) shows the three-point bending curves at room temperature (RT) for the MIL composite and monolithic Ti_3Al. Monolithic Ti_3Al exhibits only elastic behavior, and splitting-type fracture occurs immediately after the stress reaches the maximum with no indication of yielding. However, in the MIL composites, a yielding process is observed, and the stress increases progressively with increasing strains after yielding until a broad maximum appeared, followed by a gradual decrease. Accordingly, the MIL composite displays a superior fracture toughness of 40.7 MPa $m^{1/2}$ (arrester orientation), compared to that of 10.3 MPa $m^{1/2}$ for monolithic Ti_3Al. Enhancement in fracture toughness results from the suppression of formation of an unstable major crack by stress redistribution and strain delocalization, and the composite thus seems to become insensitive to flaws especially in a submicron scale.[16,17] In the case of monolithic Ti_3Al, the onset of cracking is a primary means for stress relaxation, often contributing to a premature fracture. In laminated composites, when the notch tip locates in ductile TiB_w/Ti layer, stress concentrations at the cusp are always relieved by means of plastic strain of Ti, thus making cracks hard to be produced and amplified. By contrast when it appears in brittle Ti_3Al layer, cracks are expected to be fast generated, extended, and then arrested by neighboring TiB_w/Ti layers because of plastic deformation at the crack tip, known as crack blunting. Additionally, laminated composites exhibit an improved defect toler-

ance, evidenced by an increasing critical crack length, l, as a result of strain absorption (ductile layers) and stress redistribution (laminated architecture). Kumar *et al.*[18] defined the parameter as an intrinsic attribute of composites by

$$l = \alpha \Gamma E / S^2, \qquad [3]$$

below which the fracture strength of pre-cracked materials is identical to that of a perfect crystal in spite of the presence of defects. In Eq. [3], α equals to 1.9 for Griffith-Irwin models, S is the ultimate strength, Γ is the fracture energy and qualitatively expressed as the area beneath the stress-strain curve

$$\Gamma = \int \sigma \mathrm{d}\varepsilon. \qquad [4]$$

Apparently, an increased fracture energy in laminated composites, as shown in Figure 3(b), contributes to a large magnitude of critical crack length, implying an enhanced flaws endurance compared to monolithic counterparts.

To investigate the effects of interfaces on stress redistribution and strain delocalization occurring during deformation, we undertook finite element analysis (FEA) and calculated the strain fields in both monolithic Ti_3Al and the laminated composites (without a pre-crack). All parameters and boundary conditions for the model appear in the Supplementary Materials. For the simulations, we substituted material properties of pure Ti for those of TiB_w/Ti to simplify the model. Figure 5 compares the intensity and distribution of strain fields for both monolithic Ti_3Al and Ti-Ti_3Al laminated composites. The maximum magnitude of strain for the Ti-Ti_3Al laminated composite (4.12×10^{-3}) is twice that of monolithic Ti_3Al (2.04×10^{-3}) under the same loading and boundary conditions (Figures 5(a) and (b)). The relative frequency of von Mises strain plotted in Figure 5(c) also shows that after introducing ductile layers, the average strain level of each unit increases from 3.5×10^{-4} to 7.8×10^{-4}. Also, the strain distribution curve moves to the right (to higher strains). From these results, we conclude that deformation in the Ti-Ti_3Al laminated composite should be more easily activated because of stress redistribution in the laminated architecture, which aligns with experimental measurements (a greater elongation in Figures 3 and 4).[16,17,19]

The high strain regions in the Ti-Ti_3Al laminated composite occupy greater area than those in monolithic Ti_3Al (Figures 5(a) and (b)). For instance, in monolithic Ti_3Al (Figure 5(c)), only 33 pct of units contribute to a strain of $>3.3 \times 10^{-4}$, compared with 82 pct in the laminated composite. Accordingly, under the same amount of external force, grain contributions for strain-sharing inevitably degrade in a laminated microstructure because a larger majority of grains participate into the deformation, which in turn weakens the level of stress concentrations, and also explains why the laminated composites exhibit defect insensitivity as mentioned above. With the assumption that each grain offers the same magnitude of contribution for strength and toughness, a wider dimension of deformation, after introducing a laminated architecture, imparts the observed strengthening and toughening.

Laminated composites comprises alternating ductile and brittle layers featuring periodic interfaces. When these interfaces are strongly bonded, like the *in situ* interfaces in this work, they effectively redistribute stress and inhibit strain delocalization by load transfer to adjacent layers.[20] For example, there are eight "nominal" interfaces between layers in the model of monolithic Ti_3Al (Figure 5(a)), but in fact they are imaginary and have no effect. Without real interlayer interfaces, stress concentrations inevitably arise during loading because of the limited dislocation mobility in monolithic Ti_3Al, inducing brittle fracture at low strains (~0.7 pct strain in Figure 3(b)). Figure 5(c) also shows that 6.5 pct of units in the laminated composites accommodate high strain levels ranging from 2×10^{-3} to 4.1×10^{-3}. The high strain region (gray zone in

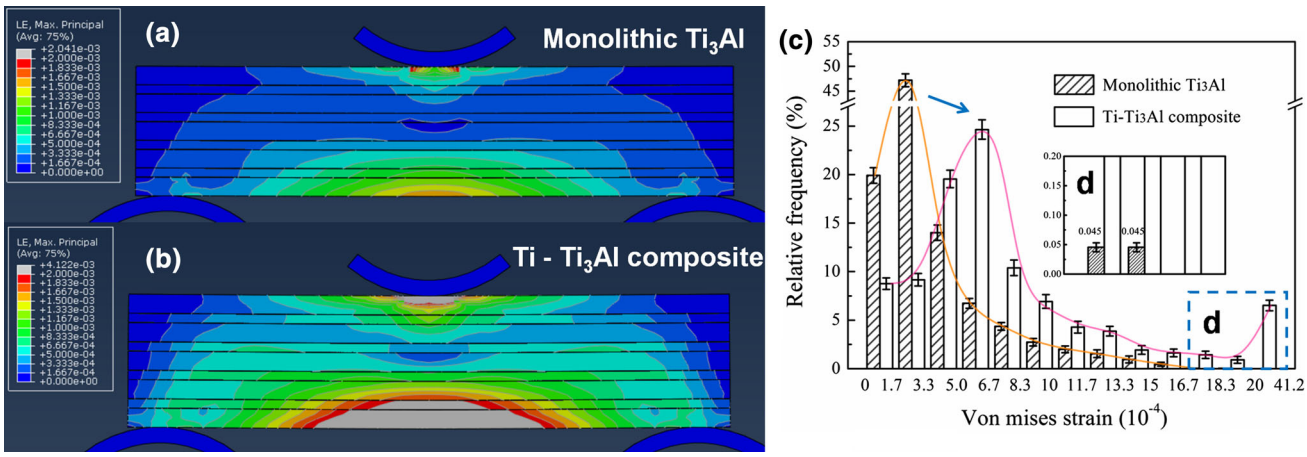

Fig. 5—Strain contour and partitioning maps during three-point bending: strain distribution of (*a*) monolithic Ti_3Al and (*b*) Ti-Ti_3Al laminated composites; (*c*) strain partitioning map. Inset in (c) is a magnified image of high strain regions.

Figure 5(b)) includes both a brittle Ti_3Al layer and a ductile Ti layer, implying that the laminated composite could withstand a relatively large strain when the brittle Ti_3Al was constrained between ductile layers.

In summary, laminated composites comprising alternating layers of Ti_3Al and TiB_w/Ti have been produced *in situ* by hot pressing and reaction annealing. The approach of using ductile TiB_w/Ti layers to impart toughness to inherently brittle Ti_3Al has been employed and explored in this work. Compared with monolithic Ti_3Al, the MIL composites exhibited superior elongation (10.6 pct) at 873 K (600 °C) and RT fracture toughness (40.7 MPa $m^{1/2}$). Tensile tests and simulations demonstrated that the laminated architecture of the microstructure imparted an ability to endure relatively large strains, and appeared to be linked to the fact that the Ti_3Al is integrated into the composite and constrained between ductile layers.

The work presented here establishes a framework for designing and producing MIL based on a wide variety of multiple-component systems (e.g., Ni-Al, Fe-Al, Nb-Al, *etc*.). The approach allows designers to sufficiently leverage the intrinsic attributes of the component phases. Such MILs and similar derivative microstructures have potential as future lightweight high-performance materials for high-temperature structural applications.

This work was financially supported by (i) the National Natural Science Foundation of China (Grant No. 51071058, 51401068), (ii) China Postdoctoral Science Foundation Funded Project (Grant No. 2013M541370), (iii) Heilongjiang Postdoctoral Fund (Grant No. LBH-Z13098), and (iv) Fundamental Research Funds for the Central University (Grant No. HIT. NSRIF. 2014001).

ELECTRONIC SUPPLEMENTARY MATERIAL

The online version of this article (doi:10.1007/s11661-015-3025-y) contains supplementary material, which is available to authorized users.

REFERENCES

1. K.L. Yang, J.C. Huang, and Y.N. Wang: *Metall. Mater. Trans. A*, 2004, vol. 35A, pp. 3803–15.
2. Y. Koizumi, T. Nakano, and Y. Umakoshi: *Acta Mater.*, 1999, vol. 47, pp. 2019–29.
3. H.M. Chan: *Annu. Rev. Mater. Sci.*, 1997, vol. 27, pp. 249–82.
4. A. Rohatgi, D.J. Harach, K.S. Vecchio, and K.P. Harvey: *Acta Mater.*, 2003, vol. 51, pp. 2933–57.
5. M.E. Launey and R.O. Ritchie: *Adv. Mater.*, 2009, vol. 21, pp. 2103–10.
6. M.E. Launey, E. Munch, D.H. Alsem, E. Saiz, A.P. Tomsia, and R.O. Ritchie: *J. R. Soc. Interface*, 2010, vol. 7, pp. 741–53.
7. K. Lu: *Science*, 2010, vol. 328, pp. 319–20.
8. Y. Kaneko, H. Sakakibara, and S. Hashimoto: *J. Mater. Sci.*, 2008, vol. 43, pp. 3931–37.
9. P.M. Anderson, J.F. Bingert, A. Misra, and J.P. Hirth: *Acta Mater.*, 2003, vol. 51, pp. 6059–75.
10. Q.W. Wang, G.H. Fan, L. Geng, J. Zhang, X.P. Cui, J.C. Pang, S.H. Qin, and Y. Du: *Intermetallics*, 2013, vol. 37, pp. 46–51.
11. X.P. Cui, G.H. Fan, L. Geng, Y. Wang, H.W. Zhang, and H.X. Peng: *Scripta Mater.*, 2012, vol. 66, pp. 276–79.
12. K. Kishida, J. Yoshikawa, H. Inui, and M. Yamaguchi: *Acta Mater.*, 1999, vol. 47, pp. 3405–10.
13. L.J. Huang, L. Geng, H.X. Peng, and J. Zhang: *Scripta Mater.*, 2011, vol. 64, pp. 844–47.
14. D.E. Alman, J.C. Rawers, and J.A. Hawk: *Metall. Mater. Trans. A*, 1995, vol. 26A, pp. 589–99.
15. P. Lhuissier, J. Inoue, and T. Koseki: *Scripta Mater.*, 2011, vol. 64, pp. 970–73.
16. T.H. Fang, W.L. Li, N.R. Tao, and K. Lu: *Science*, 2011, vol. 331, pp. 1587–90.
17. H. Kou, J. Lu, and Y. Li: *Adv. Mater.*, 2014, vol. 26, pp. 5518–24.
18. S. Kumar, M.A. Haque, and H. Gao: *Appl. Phys. Lett.*, 2009, vol. 94, p. 253104.
19. L. Lu, X. Chen, X. Huang, and K. Lu: *Science*, 2009, vol. 323, pp. 607–10.
20. J.C. Pang, G.H. Fan, X.P. Cui, A.B. Li, L. Geng, Z.Z. Zheng, and Q.W. Wang: *Mater. Sci. Eng. A*, 2013, vol. 582, pp. 294–98.